Journal of Colloid and Interface Science 668 (2024) 575–586

Contents lists available at ScienceDirect

Journal of Colloid And Interface Science

journal homepage: www.elsevier.com/locate/jcis

Regular Article

Assessing the Effect of Surface Coating on the Stability, Degradation, Toxicity and Cell Endocytosis/Exocytosis of Upconverting Nanoparticles

Lilia Arellano [a,1], Raquel Martínez [a,1,2,*], Alberto Pardo [a,*], Iago Diez [a,3], Brenda Velasco [a], Antonio Moreda-Piñeiro [b], Pilar Bermejo-Barrera [b], Silvia Barbosa [a], Pablo Taboada [a]

[a] Colloids and Polymers Physics Group, Particle Physics Department, Materials Institute (iMATUS), and Health Research Institute (IDIS), University of Santiago de Compostela, 15782 Santiago de Compostela, Spain
[b] Trace Element, Spectroscopy and Speciation Group (GETEE), Faculty of Chemistry and Materials Institute (iMATUS), University of Santiago de Compostela, 15782 Santiago de Compostela, Spain

GRAPHICAL ABSTRACT

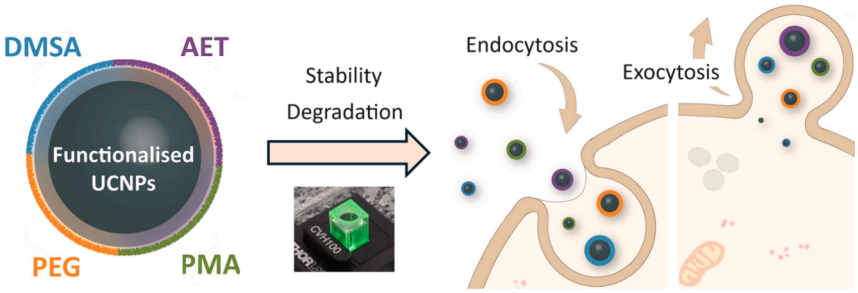

ARTICLE INFO

Keywords:
Up-converting nanoparticles
Surface coating
Stability and degradation
Endocytosis/exocytosis

ABSTRACT

Lanthanide-doped up-converting nanoparticles (UCNPs) have emerged as promising biomedical tools in recent years. Most research efforts were devoted to the synthesis of inorganic cores with the optimal physicochemical properties. However, the careful design of UCNPs with the adequate surface coating to optimize their biological performance still remains a significant challenge. Here, we propose the functionalization of UCNPs with four distinct types of surface coatings, which were compared in terms of the provided colloidal stability and resistance to degradation in different biological-relevant media, including commonly avoided analysis in acidic lysosomal-mimicking fluids. Moreover, the influence of the type of particle surface coating on cell cytotoxicity and endocytosis/exocytosis was also evaluated. The obtained results demonstrated that the functionalization of UCNPs with poly(isobutylene-*alt*-maleic anhydride) grafted with dodecylamine (PMA-*g*-dodecyl) constitutes an outstanding strategy for their subsequent biomedical application, whereas poly(ethylene glycol) (PEG) coating, although suitable for colloidal stability purposes, hinders extensive cell internalization. Conversely, surface coating with small ligand were found not to be suitable, leading to large degradation degrees of UCNPs. The

* Corresponding authors.
E-mail addresses: raquel.martinezgonzalez@physics.ox.ac.uk (R. Martínez), alberto.pardo.montero@usc.es (A. Pardo).
[1] These authors contribute equally to this work.
[2] Current address: Department of Physics, Clarendon Laboratory, University of Oxford, Parks Road, Oxford OX1 3PU, United Kingdom.
[3] Current address: Department of Physics and Astronomy, Streatham Campus, University of Exeter, North Park Road, EX4 4QL, Exeter, United Kingdom.

https://doi.org/10.1016/j.jcis.2024.04.188
Received 15 September 2023; Received in revised form 26 March 2024; Accepted 26 April 2024
Available online 27 April 2024

analysis of particle' behavior in different biological media and *in vitro* conditions here performed pretends to help researchers to improve the design and implementation of UCNPs as theranostic nanotools.

1. Introduction

Lanthanide-doped up-converting nanoparticles (UCNPs) have been intensively studied in recent years thanks to their ability to convert near-infrared (NIR) excitation into ultraviolet (UV) and visible (Vis) emissions [1–3]. In the most typical design, UCNPs consist of $NaYF_4$ matrices doped with Yb^{3+} ions as sensitizers that collect and transfer energy to co-doped lanthanide ions (*e.g.* Er^{3+}, Tm^{3+}) [4–6]. These activator ions provide intermediate metastable *4f* excited states, which can generate effective up-converting luminescent emission upon sequential absorption of multiple low-energy photons into the energy levels of lanthanide dopants. Due to the long-lived intermediate energy states of lanthanide ions, UCNPs display enhanced properties compared to other luminescent materials, such as semiconductor quantum dots or organic dyes, in terms of luminescence lifetimes or resistance to photobleaching [7,8]. The intense tunable reemissions from UCNPs upon the absorption of NIR radiation allow deep and sharp tissue penetration, having been exploited in the biomedical field for detection [9], bioimaging [10], drug delivery [11], or photodynamic therapy [12].

Nevertheless, in view of the increasing use of UCNPs in biological applications, their potential dissemination, interactions with human cells/tissues, and potential harmful side effects must be considered in their design [13,14]. In this sense, it is worth mentioning the existence of several previous works that demonstrate the risks associated with the use/exposition of/to rare earth elements present in the structure of UCNPs [15–18]. In the specific case of nanoparticulated systems, the degradation of UCNPs involves important releases of F^-, Y^{3+} and Yb^{3+} ions, giving rise to the presence of insoluble salts of lanthanide phosphates upon incubation in phosphate buffers [19]. To shield their interaction with the surrounding biological environment and avoid unwanted degradation while providing colloidal stability and biocompatibility, the surface chemistry of UCNPs appears as an essential factor [1,13,20]. Many different types of ligands and coatings have been proposed, ranging from small molecules and surfactants (*e.g.* ethylenediamine tetra(methylene phosphonic acid)) [16,21], to polymers (*e.g.* poly (ethylene glycol) (PEG)) [22–24], and inorganic coatings (*e.g.* silica) [24,25]. However, most commonly used coatings were unable to hinder the degradation of the UCNPs in biologically relevant media such as acidic lysosomal-mimicking fluids, thus varying their properties and compromising cell viability.

Prompted by these findings, in this work we designed highly crystalline UCNPs and rendered them dispersible in biological media by means of different nanoparticle surface coatings. Besides evaluating a typical capping agent such as PEG, three other less explored coatings were analyzed: a polymer as poly(isobutylene-*alt*-maleic anhydride) modified by grafting with dodecylamine (PMA-*g*-dodecyl); and two small ligands such as *meso*-2,3-dimercaptosuccinic acid (DMSA) and 2-aminoethyl dihydrogen phosphate (AET). The evaluation of PMA-*g*-dodecyl was motivated by its proven excellent performance as coating in both magnetic and gold nanostructures [26–28], being its use with rare earth-based nanoparticles still very limited [29]. UCNPs functionalization with DMSA was analyzed despite its low suitability a priori owing to its small molecular size; nevertheless, in the basis of an own previous work, this coating rendered large ferrimagnetic nanostructures, which are prone to aggregate, highly stable in biological media [30]. Finally, AET coating was selected as an alternative low-molecular-weight ligand to establish a direct comparison with DMSA [29,31,32]. The influence of these nanoparticle coatings on the colloidal stability, degradation, biocompatibility, and cell endocytosis/exocytosis of UCNPs was exhaustively evaluated.

2. Experimental

2.1. Materials

The detailed list of materials can be found in Supplementary Information.

2.2. Synthesis of UCNPs

Highly-monodisperse cubic-shaped β-$NaYF_4$:$Yb_{0.18}Er_{0.02}$ UCNPs were obtained by mixing 1.60 mmol of $YCl_3{\cdot}6H_2O$, 0.36 mmol of $YbCl_3{\cdot}6H_2O$ and 0.04 mmol of $ErCl_3{\cdot}6H_2O$ with 33 mmol of oleic acid (OA) and 30.0 mL of 1-octadecene. The solution was heated to 150 °C and keep for 1 h under vacuum to eliminate oxygen and water traces. After cooling down to room temperature, 8 mmol of NH_4F and 5 mmol of NaOH in 10 mL of methanol were added, forming a translucent yellow-white solution after 30 min stirring at 50 °C. The methanol was evaporated by increasing the temperature to 80 °C under vacuum and, after 20 min, the solution became transparent. Then, the mixture was heated at 7 °C·min^{-1} up to 300 °C under N_2 atmosphere and kept at reflux for 1 h. The UCNPs were precipitated by adding methanol and centrifuging (2000 rcf, 10 min) and finally redispersed in chloroform [33,34]. The composition, size, and morphology of the UCNPs were tuned by modifying the ratios between lanthanide precursors and OA (see amounts of reagents used for the synthesis of each type of UCNPs in Supplementary Information: Table S1).

2.3. Aqueous phase transfer of UCNPs

AET, DMSA and PEG functionalization: 20 mg of dried OA-capped UCNPs were dispersed in 5 mL of 1.0 mM HCl for 3 h. The remaining OA was extracted with 5 mL diethyl ether (three times). Next, the UCNPs were precipitated by adding acetone and centrifuging (1000 rcf, 15 min) and redispersed in 5 mL of AET, DMSA or PEG aqueous solutions (5 mg·mL^{-1}) under sonication for 15 min. PMA functionalization: PMA was initially modified with dodecylamine (PMA-*g*-dodecyl) as reported elsewhere [35]. Then, 1 mL of OA-capped UCNPs at 5 mg·mL^{-1} was mixed with 1.5 mL of PMA-*g*-dodecyl at 0.25 M (monomer concentration), adding additional 5 mL of chloroform. The solvent was slowly evaporated in a rotavap and dried UCNPs were redispersed in 2 mL of 0.10 M sodium borate buffer (SBB) at pH 12. In all cases, the obtained UCNP@AET, UCNP@DMSA, UCNP@PEG or UCNP@PMA were collected by centrifugation (21000 rcf, 30 min) and washed three times to remove the excess of surface ligands.

2.4. Colloidal stability and degradation of UCNPs

Spherical-shaped β-$NaYF_4$:$Yb_{0.18}Er_{0.02}$ UCNPs with the different surface coatings were dispersed in SBB, Dulbecco's modified Eagles's medium (DMEM), DMEM supplemented with 10 % (v/v) of fetal bovine serum (FBS), phagolysosomal mimicking medium (PSF), or PSF supplemented with 1 mM KF. The variations of ζ-potential and hydrodynamic size values were measured for 4 days. The degradation of UCNPs was evaluated by quantifying the released F^- ions and the variation of luminescence emission intensity. For F^- release studies, 1 mg·mL^{-1} of UCNPs were dispersed in the selected medium at 37 °C and incubated for the analyzed time. Afterwards, the UCNPs were collected by centrifugation (15000 rcf, 5 min), followed by ultrafiltration (MW 30 kDa) to eliminate any remaining particle. A potentiometric system with fluoride-ion-selective electrode (Methrom, Titrator Excellence T7) was used to quantify the amount of F^- in the supernatants. Experimental

details about luminescence emission measurements can be found in Supplementary Information. The experiments were performed in triplicate.

2.5. Characterization

Details of the characterization techniques can be found in Supplementary Information.

2.6. In vitro cell assays: Cytotoxicity and internalization of UCNPs

Tumoral human cervical HeLa cells, murine Balb/3T3 fibroblasts and Raw 264.7 murine macrophages were purchased from Cell Biolabs (San Diego, CA, USA) and grown at standard culture conditions (5 % CO_2 at 37 °C) in DMEM supplemented with 10 % (v/v) FBS, 2 mM L-glutamine, 1 % (v/v) penicillin/streptomycin, 1 mM sodium pyruvate, and 0.1 mM nonessential amino acids. The *in vitro* cytotoxicity UCNPs was evaluated by means of the CCK-8 cytotoxicity assay. These cell viability data were complemented by measuring the cytokine release from macrophages, an indication of the inflammatory stress supported by cells which may lead to apoptosis. On the other hand, the uptake and internalization of UCNPs within HeLa cells was monitored by confocal microscopy. In addition, the influence of the UCNPs surface coating on cell internalization and clearance was also quantified by means of inductively coupled plasma mass spectrometry (ICP-MS). Experimental details of these procedures can be found in Supplementary Information.

3. Results and discussion

3.1. Synthesis and physical characterization of UCNPs

In a typical synthetic procedure (see Experimental Section for details), monodisperse UCNPs were obtained through a bottom-up thermal decomposition method [36–38]. The morphology of the nanostructures can be controlled by varying the molar ratio between OA and lanthanide chlorides (Ln^{3+}) in precursor mixtures. In this way, we synthesized UCNPs based on $NaYF_4$ matrices doped with 18 % Yb^{3+} and 2 % Er^{3+} ($NaYF_4$:$Yb_{0.18}$:$Er_{0.02}$) displaying cubic, rod and spherical shape at OA:Ln^{3+} molar ratios between 16.5 and 21.5 (Fig. 1A-D; Table S1 in Supplementary Information).

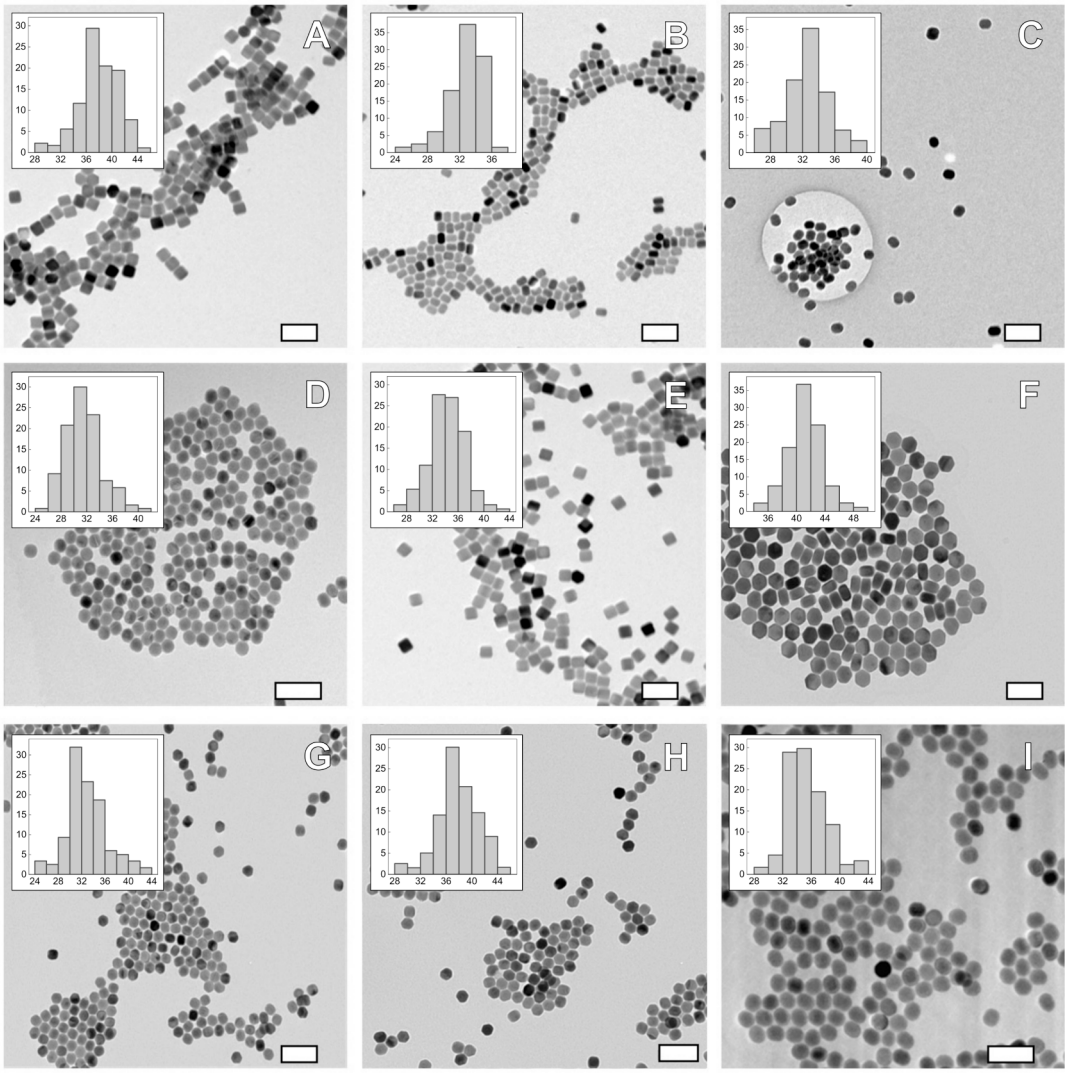

Fig. 1. Transmission electron microscopy (TEM) images of $NaYF_4$:$Yb_{0.18}$:$Er_{0.02}$ UCNPs with: (A) cubic, (B-C) rod, and (D) spherical morphology prepared at OA:Ln^{3+} molar ratio of 16.5, 19.0, 20.0 and 21.5, respectively. $NaYF_4$:$Yb_{0.18}$:$Tm_{0.005}$ UCNPs with (E) cubic, (F) mix rod/hexagonal, and (G-H) spherical morphology prepared at OA:Ln^{3+} molar ratio of 16.5, 19.0, 20.0 and 21.5, respectively. (I) $NaGdF_4$:$Yb_{0.18}$:$Er_{0.02}$ nanospheres prepared at OA:Ln^{3+} molar ratio of 19.0. Insets show statistical frequency (%) *vs.* size (nm) distributions (edge length for cubes, diameter for spheres and hexagons; length for rods; width distributions of rod-shaped UCNPs can be found in Fig. S1 in Supplementary Information). Scale bars 100 nm.

The different morphology of the designed UCNPs was attributed to the effect of the amount of OA chains incorporated in the synthetic process on the bottom-up growth mechanism of the particles. For a hexagonal $NaYF_4$ lattice (determined by X-ray diffraction (XRD), see below), the area of the $\{10\bar{1}0\}$ facet exceeds that of the {0001}, so that the latter will have a higher surface energy and a faster growth rate. Thus, when the OA:Ln^{3+} molar ratio is low, OA molecules would preferentially adsorb onto the {0001} facets, giving rise to nanocubes (Fig. 1A). With further increases in the OA:Ln^{3+} molar ratio, the number of OA molecules reaches saturation on the {0001} facet and becomes progressively larger on the $\{10\bar{1}0\}$ one, with larger surface area; in this manner, the growth velocity becomes progressively similar along the {0001} and $\{10\bar{1}0\}$ directions, giving rise firstly to nanorods (Fig. 1B-1C) and, then, to nanospheres when the velocity is equal in both facets (Fig. 1D) [39].

On the other hand, and despite the main focus of this work was to analyze the effect of the surface coating of UCNPs on their biological performance, we have also demonstrated the versatility of our strategy by synthesizing UCNPs with different compositions. Thus, the emission spectrum of the UCNPs was selectively tuned by incorporating Tm^{3+} instead of Er^{3+} as doping activator ions ($NaYF_4$:$Yb_{0.18}$:$Tm_{0.005}$). The substitution of 2 % Er^{3+} by 0.5 % Tm^{3+} slightly decreases the OA:Ln^{3+} ratios at which the morphology transitions take place, being this attributed to the already established effect of lanthanide activator and extent of doping on the structure and physicochemical characteristics of the resulting UCNPs [40]. In this way, cubic-shaped, a mix of rods and hexagons and spherical-shaped UCNPs were obtained at OA:Ln^{3+} ratios of 16.5, 19.0 and 20.0–21.5, respectively (Fig. 1E-H). Additionally, UCNPs composed of Gd^{3+} instead of Y^{3+} as constituent of the host matrices obtaining spherical-shaped $NaGdF_4$:$Yb_{0.18}$:$Er_{0.02}$ UCNPs at a

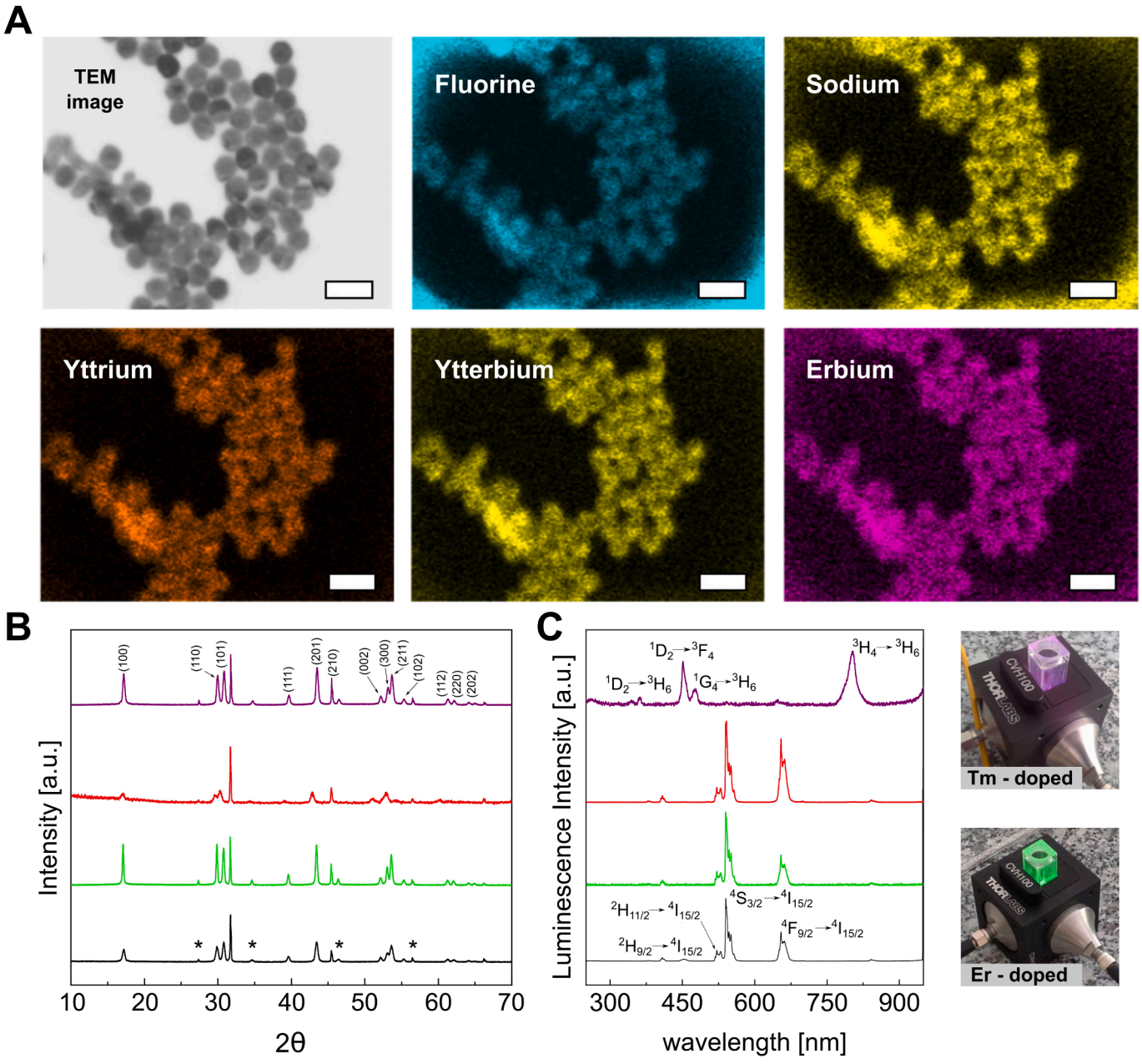

Fig. 2. Structural and luminescence characterization of UCNPs. (A) EDX mapping analysis of spherical-shaped $NaYF_4$:$Yb_{0.18}$:$Er_{0.02}$ UCNPs (Scale bars 50 nm). (B) XRD patterns and (C) luminescence spectra upon 980 nm-laser excitation of cubic- (black) and spherical-shaped (green) $NaYF_4$:$Yb_{0.18}$:$Er_{0.02}$, $NaGdF_4$:$Yb_{0.18}$:$Er_{0.02}$ (red), and NaYF4:$Yb_{0.18}$:$Tm_{0.005}$ (purple) UCNPs. Photographs in (C) show the bare-eye emissions at different wavelengths of thulium- and erbium-doped UCNPs.

fixed OA:Ln^{3+} molar ratio of 19.0 (Fig. 1I). However, as previously mentioned, these nanostructures were designed only as a proof of concept to demonstrate the versatility of our strategy to obtain UCNPs with different sizes, morphologies and/or compositions. An exhaustive study of their properties and applications will be the subject of a forthcoming publication.

ICP-MS measurements confirmed the formation of the host matrices based on yttrium or gadolinium and the successful incorporation of the different sensitizer and activator ions within them according to the established precursor ratios (Additional File 1: Table S2). Moreover, energy-dispersive X-Ray (EDX) analysis was also performed for spherical-shaped $NaYF_4$:$Yb_{0.18}$:$Er_{0.02}$ UCNPs as example, confirming the presence of the different constitutive elements within the crystal matrices (Fig. 2A). On the other hand, XRD characterization showed that all the synthesized UCNPs display β-hexagonal crystal lattices, which agrees with their excellent luminescent emissions (Fig. 2B; see also Fig. S2 in Supplementary Information, where all the spectrums are represented). The presence of some minor residual peaks in XRD spectra (denoted with *) indicate the existence of small parts of particles' structure with α-cubic crystallographic phase, while the peaks at *ca.* 32° arise from the presence of remaining OA chains. In terms of photoemission properties, $NaYF_4$:$Yb_{0.18}$:$Er_{0.02}$ UCNPs showed main emissions at 524 nm ($^2H_{11/2} \rightarrow {}^4I_{15/2}$; green), 540 nm ($^4S_{3/2} \rightarrow {}^4I_{15/2}$; green), and 654 nm ($^4F_{9/2} \rightarrow {}^4I_{15/2}$; red) upon excitation with a non-collimated 980 nm laser beam. $NaYF_4$:$Yb_{0.18}$:$Tm_{0.005}$ UCNPs displayed emission bands at 360 nm ($^1D_2 \rightarrow {}^3H_6$; UV), 451 nm ($^1D_2 \rightarrow {}^3F_4$; violet), 476 nm ($^1G_4 \rightarrow {}^3H_6$; blue), and 840 nm ($^3H_4 \rightarrow {}^3H_6$; NIR), respectively, while $NaGdF_4$:$Yb_{0.18}$:$Er_{0.02}$ UCNPs showed similar emission lines as those of $NaYF_4$:$Yb_{0.18}$:$Er_{0.02}$ ones, as expected given their same activator element (Fig. 2C).

3.2. Surface modification of UCNPs

For the intended biological applications of UCNPs, it is required to provide them with long-term colloidal stability in biological media while preventing their aggregation and/or degradation. For this purpose, we performed four different surface coatings of the designed UCNPs, taken spherical-shaped $NaYF_4$:$Yb_{0.18}$:$Er_{0.02}$ nanostructures as a model for their subsequent evaluation in various media of biological interest. The UCNPs with the different stabilizing agents were denoted as UCNP@AET, UCNP@DMSA, UCNP@PEG and UCNP@PMA.

As expected, non-modified UCNPs with OA chains on their surface obtained by thermal decomposition were highly agglomerated when trying to disperse in water, displaying an average hydrodynamic size of 438 ± 47 nm (Fig. 3A). After the functionalization processes, the successful attachment of the different ligands to the UCNPs surface was evaluated by Fourier-transform infrared spectroscopy (FTIR) (Fig. 3B; see the bonds associated with each band in Fig. S3 in Supplementary Information) [28,30,41–45]. Furthermore, the subtle changes observed in the particle surface charge also confirmed the successful attachment of the coating molecules to the UCNPs, displaying average ζ-potential values of −7.5 ± 1.9 (UCNP@AET), –23.8 ± 2.6 (UCNP@DMSA), −14.7 ± 1.5 (UCNP@PEG), and –22.5 ± 1.9 mV (UCNP@PMA). Thermogravimetric analysis (TGA) was performed to establish the weight percentage of the nanostructures attributed to the coating layers, observing that small ligands such as DMSA represent only *ca.* 12 % of weight of functionalized UCNPs while this percentage increases up to *ca.* 20 % in the case of larger polymeric structures such as PMA-*g*-dodecyl (Fig. S4 in Supplementary Information). Finally, dynamic light scattering (DLS) data showed that all the surface coatings provided the UCNPs with an initial high stability in water, displaying similar hydrodynamic sizes ranging from 104 to 110 nm (Fig. 3A).

3.3. Colloidal stability of UCNPs in biological media

The colloidal stability of coated UCNPs was evaluated by monitoring their hydrodynamic size and ζ-potential upon 48 h incubation in two complex biological media: DMEM supplemented with 10 % (v/v) FBS and PSF. Thus, UCNP@AET displayed an initial hydrodynamic size of 106 ± 8 nm in supplemented DMEM, which slightly increased within the first 12 h of incubation up to 122 ± 6 nm, probably due to a combination of protein adsorption and certain particle destabilization caused by the high ionic strength of the medium. Further incubation led to remarkable particle size increasing up to 139 ± 9 nm. In the case of UCNP@DMSA, the initial hydrodynamic size was 102 ± 7 nm, displaying a starting ζ-potential of −13.3 ± 0.7 mV. The hydrodynamic size was observed to slightly increase along incubation up to 117 ± 5 nm, probably as consequence of the formation of a thin protein corona. No appreciable variation in their surface charges was noted except at 48 h of incubation, for which the ζ-potential slightly increased to −11.7 ± 0.5 mV. For UCNP@PEG, the initial hydrodynamic size and ζ-potential values (101 ± 8 nm and −13.4 ± 1.0 mV, respectively) barely changed during the incubation time thanks to the steric hindrance provided by this polymer. The surface charge of UCNP@PEG was slightly negative as a consequence of the delocalization of electron pairs in the ether bond of PEG monomers, but contribution of some adsorbed protein molecules onto the particles' surface cannot be completely neglected [46,63]. UCNP@PMA showed an initial hydrodynamic size of 106 ± 9 nm and ζ-potential value of −14.3 ± 1.8 mV, and both magnitudes barely varied during incubation time, which denoted an outstanding stability of UCNP@PMA in this medium (Fig. 3C).

On the other hand, when the incubation was performed in PSF (see composition in Table S3 in Supplementary Information), important variations in the colloidal stability of the coated UCNPs were noted (Fig. 3D). UCNP@AET hydrodynamic sizes were observed to largely increased from the beginning of the incubation process up to 507 ± 48 nm after 48 h, denoting a strong aggregation consequence of the experienced degradation, as shown later. UCNP@DMSA also underwent a remarkable increase on their hydrodynamic size during incubation from up 202 ± 19 nm, with ζ-potential varying from −5.1 ± 0.5 to −11.9 ± 1.8 mV. This denoted that DMSA coating provided better stability than AET, particularly at short incubation times, but both ligands are not suitable to achieve the desired protection of UCNPs in PSF. UCNP@PEG and UCNP@PMA showed high stability in acidic media, with hydrodynamic sizes within the range 110–125 nm during incubation and no signs of aggregation. On the other hand, progressive reductions in their surface potentials were observed up to −9.7 ± 0.6 mV and −14.6 ± 1.4 mV, respectively, thus providing certain electrostatic stability in addition to polymeric steric hindrance. (Fig. 3D). In summary, PEG and PMA-*g*-dodecyl coatings were able to provide UCNPs with high stability under some cell mimicking conditions, whereas DMSA and, especially, AET coatings become more unstable and were not able to hinder the aggregation of ceramic UCNPs.

3.4. UCNPs degradation

In addition to the two media in which we previously assessed colloidal stability, the degradation study of UCNPs was expanded to other two simpler media: non-supplemented DMEM and SBB. Moreover, to analyze the effect of the presence of added F^- ions on the degradation of UCNPs, we also studied PSF media supplemented with 1 mM KF. In this regard, it is worth mentioning that fluoride anions are essential in human body, being a micronutrient necessary to, for instance, prevent dental cavities and promote healthy bone growth [47,48].

As expected from previous studies [14,21], the designed UCNPs were low-degraded when dispersed in SBB medium, displaying reduced releases of F^- ions and low decays on luminescence intensities even after 96 h incubation (Fig. 3E(i)-3F(i)). This low degradation degree was especially remarkable for UCNP@PMA and UCNP@PEG. A similar behavior was observed when the UCNPs were dispersed in non-supplemented DMEM (Fig. 3E(ii)-3F(ii)). In the case of DMEM-FBS medium, UCNP@PMA and UCNP@PEG maintained a low degradation

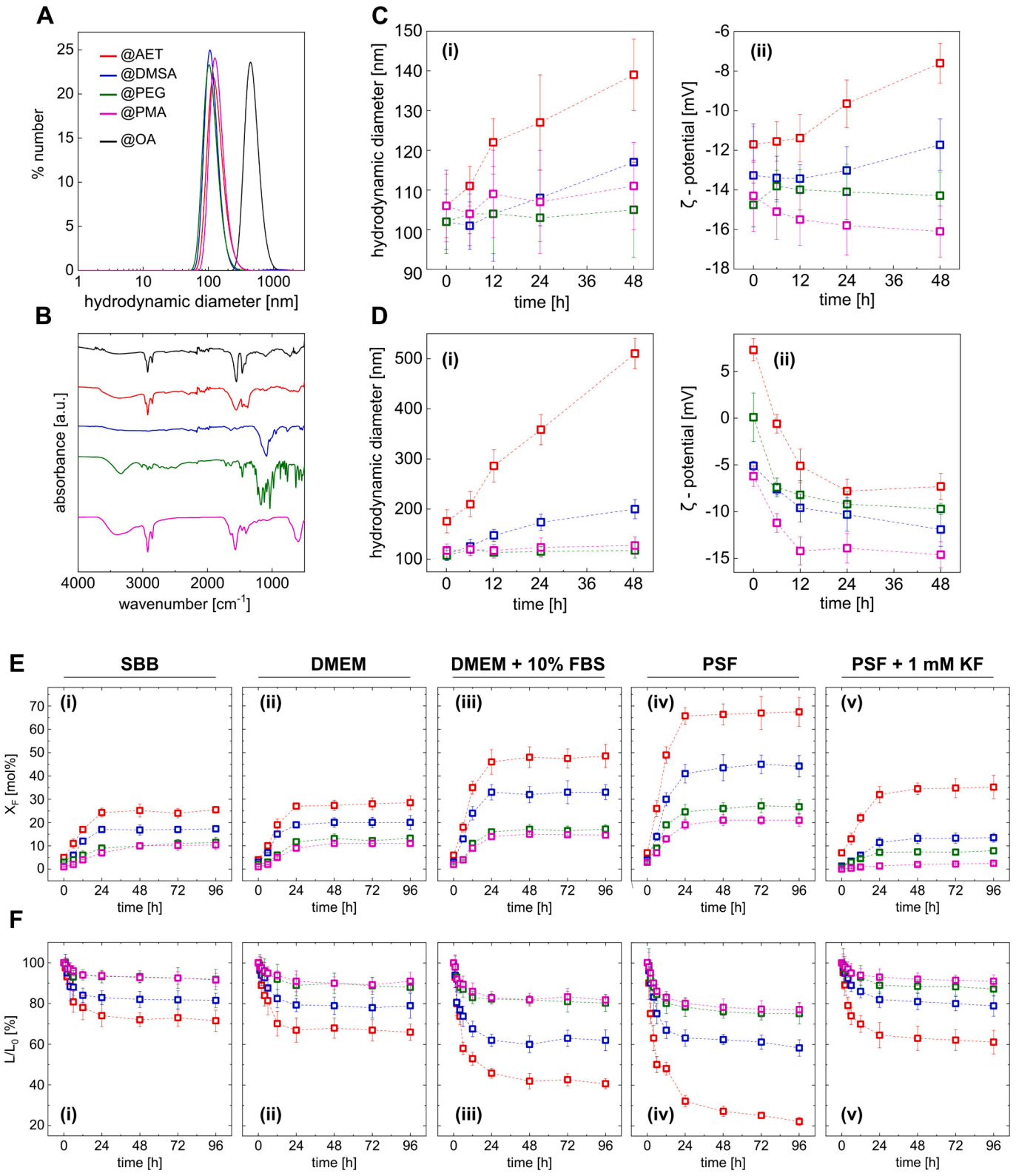

Fig. 3. Colloidal stability and degradation of the UCNPs in biological media. (A) Population hydrodynamic diameter distributions and (B) FTIR spectra of spherical-shaped $NaYF_4$:$Yb_{0.18}$:$Er_{0.02}$ UCNPs coated with OA (black), AET (red), DMSA (blue), PEG (green), and PMA-*g*-dodecyl (magenta) dispersed in water after 0 h incubation at 37 °C. Colloidal stability of the functionalized UCNPs when: (C) incubated in DMEM + 10 % (v/v) FBS analyzed in terms of (i) hydrodynamic size and (ii) ζ-potential variation; (D) incubated in PSF analyzed in terms of (i) hydrodynamic size and (ii) ζ-potential variation. (E) Fraction of F^- released from $NaYF_4$:$Yb_{0.18}$:$Er_{0.02}$ UCNPs (X_F) upon incubation in (i) SBB, (ii) DMEM, (iii) DMEM + 10 % (v/v) FBS, (iv) PSF, and (v) PFS + 1 mM KF. (F) Luminescence decay ratio of $NaYF_4$:$Yb_{0.18}$:$Er_{0.02}$ UCNPs (L/L_0) upon incubation in (i) SBB, (ii) DMEM, (iii) DMEM + 10 % (v/v) FBS, (iv) PSF, and (v) PFS + 1 mM KF. UCNPs concentration was 10 μg·mL^{-1} in all cases in (E) and (F). Polydispersity index associated with each DLS measurement can be found in Table S4 in Supplementary Information.

degree, but it increased markedly in the case of the particles coated with DMSA and, especially, AET (Fig. 3E(iii)-3F(iii)), being this fact attributed to the loss of stability derived from the larger adsorption of proteins on UCNPs' surfaces. On the other hand, more important transformations of UCNPs occurred when incubated in PSF, observing large releases of F^- ions and notable decays on luminescence signals, being these particularly stronger for UCNP@AET (Fig. 3E(iv)-3F(iv)). Interestingly, the presence of added F^- ions in the PSF medium strongly decreased the degradation degree of the UCNPs (Fig. 3E(v)-3F(v)), in agreement with the fact that the maximum F^- concentration is determined by its

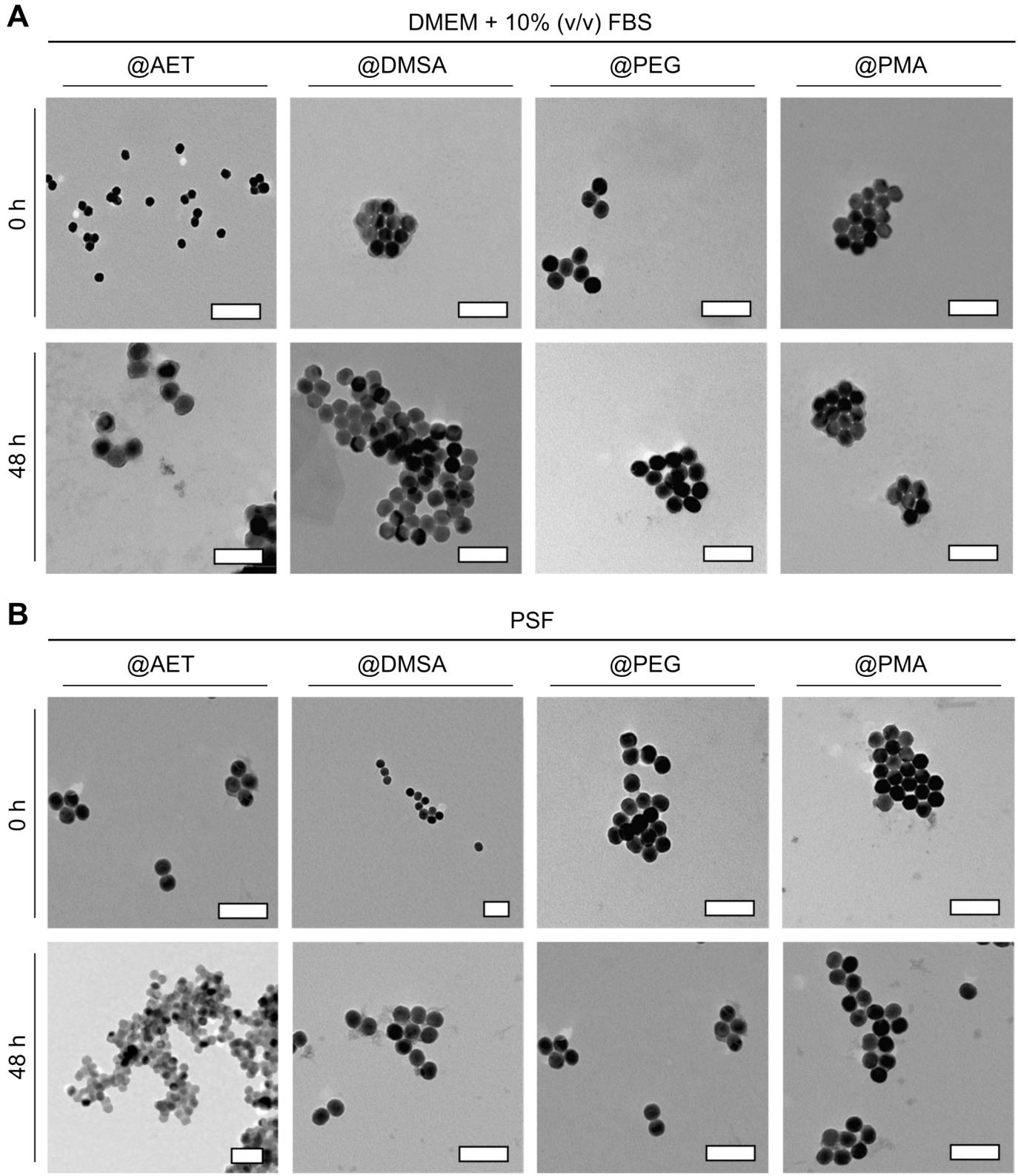

Fig. 4. Microscopy analysis of UCNPs degradation. TEM images of spherical-shaped $NaYF_4$:$Yb_{0.18}$:$Er_{0.02}$ UCNPs coated with AET, DMSA, PEG and PMA-*g*-dodecyl upon 0–48 h incubation in (A) DMEM + 10 % FBS and (B) PSF. Scale bars 100 nm.

equilibrium value [19,49,50].

The observed relationship between the loss of luminescence and F^- release from UCNPs is consistent with previous reports [19,51], being derived from the key role of particles crystallinity on the intensity of their luminescence emissions. However, luminescence signals can be also affected by flocculation of UCNPs or heterogeneous precipitation of other materials on the particles' surface (*e.g.* phosphates in the case of PBS buffers) [52]. The effect of particle's concentration was also briefly evaluated using UCNP@AET, observing larger degradation degrees in diluted dispersions (Fig. S5 in Supplementary Information). This fact might be considered when preparing dispersions with low circulating concentrations in the order of few tens/hundreds of μg of UCNPs per mL, such as those typically used in biological applications [53].

TEM images were also acquired to evaluate the structural and physicochemical alterations of the diverse types of functionalized UCNPs when incubated in DMEM supplemented with FBS and PSF (Fig. 4). In the case of DMEM-based media, it was observed that the previously determined luminescence emission losses and large release of F^- ions from UCNP@AET resulted in a low structural stability of the particles. UCNP@DMSA showed a remarkably lower degradation degree, being only noted some particle agglomeration. UCNP@PEG and UCNP@PMA maintained their well-defined morphology, in agreement with their lower release of F^- ions to the medium, thus confirming the best protection against degradation provided by these coatings (Fig. 4A). Similarly, TEM analysis confirmed the important alteration of UCNP@AET dispersed in PSF, with a partial loss of morphology and the formation of intertwined or agglomerated particle chains after 48 h of incubation. In the case of UCNP@DMSA, some particle surface alterations could be observed after incubation, being these variations more important than those previously observed when dispersed in DMEM-based medium. In the case of UCNP@PEG and UCNP@PMA, they again maintained high degrees of monodispersity upon 48 h incubation in PSF (Fig. 4B).

In summary, we have demonstrated that PEG and, more especially, PMA-*g*-dodecyl coatings, provided UCNPs with high colloidal stability and resistance to degradation. In particular, PMA-*g*-dodecyl coatings preserved the luminescence intensities of UCNPs above 90 % and 80 % of original values after 96 h incubation in DMEM-based media and PSF, thus constituting a significantly higher protector against particles' degradation than other previously proposed surface modifications [52,54]. The excellent performance of PMA-*g*-dodecyl coatings to render different nanostructured materials highly stable in aqueous media [26,28] is derived from the mechanism used to attach the polymeric molecules. In this sense, it was reported that surface coatings based on the deposition of additional amphiphilic layers, maintaining the original hydrophobic layers (*i.e.* polymer coating), gave rise to UCNPs with reduced non-radiative quenching by aqueous media in comparison with those that were rendered water-dispersible *via* ligand exchange processes [23].

We want to highlight that, unlike most previous works in which stability studies were very limited to PBS or DMEM-based media, the evaluation of the behavior of UCNPs in PSF here performed provided important information about the optimal coating of UCNPs. Thus, although the coatings with AET and DMSA rendered UCNPs with reasonably good protection when incubated in the most common media, their performance drastically dropped when they were evaluated in PSF. This fact limits the use of these surface modifications in applications that require the cellular internalization of UCNPs. To the best of our knowledge, the behavior of UCNPs in PSF media has hardly been analyzed before [16], being this stability/degradation study a valuable guide for the design nanostructures with cell internalization potential.

3.5. *In vitro evaluation of UCNPs*

Thanks to their outstanding optical properties, UCNPs are being widely studied as potential nanotools for multimodal imaging and photodynamic therapy, amongst other applications. However, the potential harmful effects due to particle biotransformation or inherent component toxicity might preclude their translation to the clinics. To determine whether the UCNPs with the performed coatings are biocompatible, the viability of Balb/3T3 murine fibroblasts and human cancerous HeLa cells was assessed after 24–48 h of UCNPs administration by means of CCK-8 toxicity assays.

As observed in Fig. 5A-C, all types of coated UCNPs were non-toxic for both cell lines after 24 h of incubation, with viabilities above 80 %. After 48 h, UCNPs showed a more remarkable concentration- and coating-dependent toxicity (Fig. 5B-D). Thus, cell viabilities larger than 80 % were only achieved at particles' concentrations below 9.1 and 36 $\mu g \cdot mL^{-1}$ when HeLa and Balb/3T3 cells were incubated in the presence of UCNP@AET. In particular, this kind of particles showed the lowest observed cell viability, reaching 41 % after 48 h of incubation in HeLa cells at the highest analyzed concentration (Fig. 5B). This behavior was attributed to the large release of F^- ions from the structure of UCNP@AET that can be harmful for cells, particularly for cancerous ones, which have a more accelerated metabolism. In the case of UCNP@DMSA, the critical concentration above which cell viabilities decreased below 80 % was 36 $\mu g \cdot mL^{-1}$ in both cell types. For their part, UCNP@PEG and UCNP@PMA showed high cytocompatibility, with viabilities above 90 % for all the analyzed concentrations in both cell lines (Fig. 5A-D).

The cytocompatibility of UCNPs was also evaluated by measuring the release of IL-6 and TNF-α cytokines from RAW 264.7 murine macrophages upon 24 h incubation. Although cytokine production is not directly related to cell mortality, it is a well-established indication of inflammatory stress supported by cells, which may lead to their apoptosis. The obtained results confirmed previous CCK-8 viability data, with UCNP@PMA and UCNP@PEG showing similar cytokines release than control cells. UCNP@DMSA and UCNP@AET reached much larger values, which confirm the high inflammatory stress induced by these typologies of particles in the cells, especially in the case of UCNP@AET at large concentrations. Bare UCNPs were also evaluated, observing cytokines release values up to six times those observed in control cells due to the low biological stability and the consequent high stress induced by these non-functionalized nanoparticles (Fig. S6 in Supplementary Information).

Next, the internalization of UCNPs within HeLa cells was monitored through confocal microscopy. It is well-known that the quantum yield from upconversion in UCNPs is highly dependent on their surface chemistry, this being a factor that can distort the evaluation of the internalization of UCNPs with different coatings through the study of confocal microscopy images. However, the previously performed evaluation of their luminescence in biological media (Fig. 3F) allowed the use of emission intensity observed on confocal images to qualitatively compare the internalization degrees of the different particles. Thus, the internalization degrees of UCNP@PEG, UCNP@PMA and UCNP@DMSA in the first 24 h incubation can be directly compared based on the luminescence observed on the confocal images (similar emission profiles), while the strong decays on the luminescence of UCNP@AET must be considered on the analysis.

Fig. 5E shows a strong luminescence inside the cytoplasm of HeLa cells along the first 6 h of incubation for UCNP@AET, which denotes a large cell uptake. The luminescence pattern indicates that the particles were aggregated within the cells, probably inside endo/lysosomes due to their lower pH, which would agree with colloidal stability data. However, after 24 h incubation the luminescence signals strongly decreased due to UCNPs degradation. The biological-induced removal of AET on the particle surface can be the origin of such degradation process since similar phosphate-based coatings have been demonstrated to be unable to protect the particles under abiotic and biotic conditions [16]. On the other hand, UCNP@DMSA and UCNP@PEG were also initially internalized within the cells, but at much lower extents than UCNP@AET, due to the positive surface charge of these last ones in

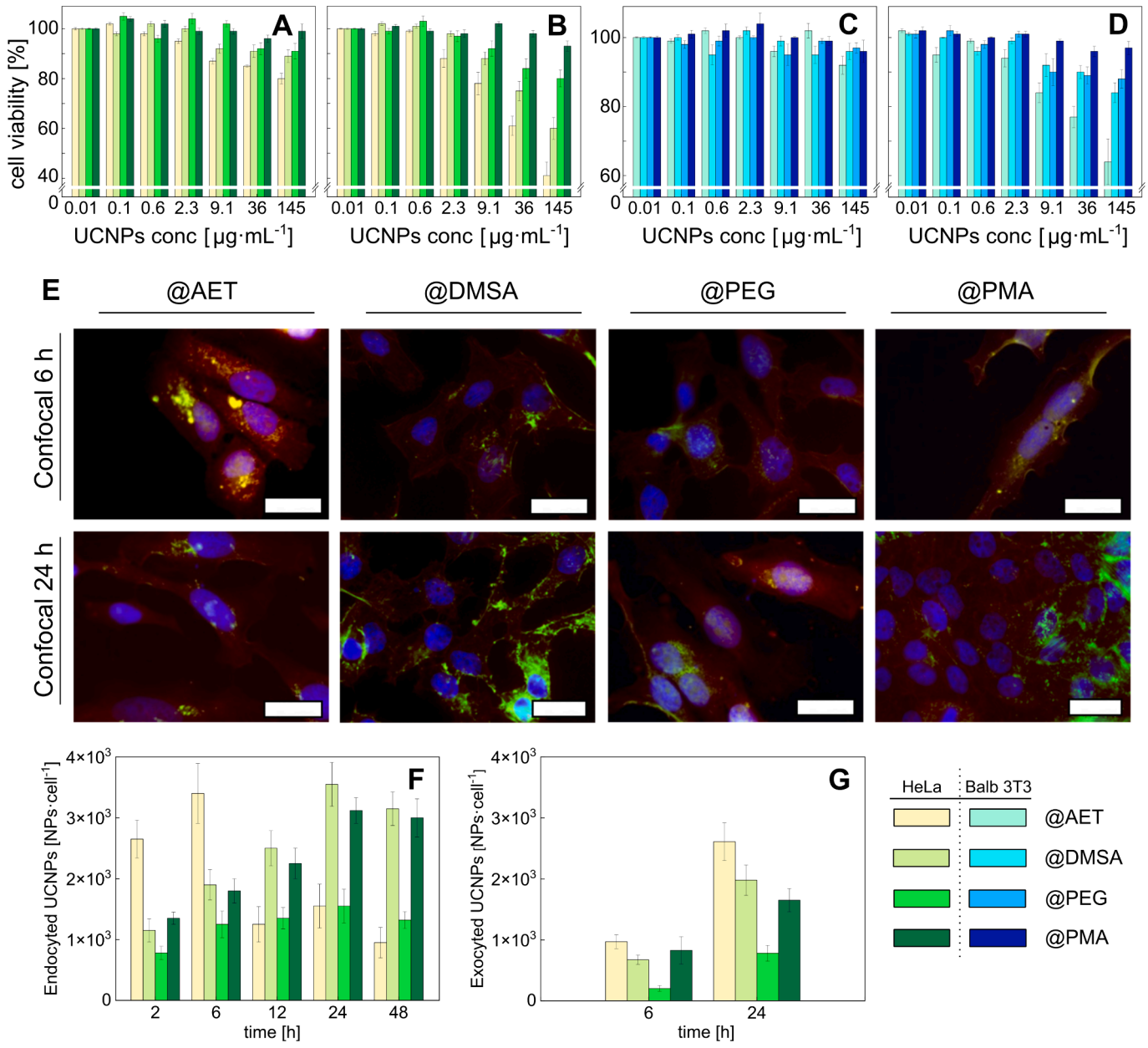

Fig. 5. Cell viability, endocytosis, and exocytosis of spherical-shaped $NaYF_4$:$Yb_{0.18}$:$Er_{0.02}$ UCNPs. Viability of HeLa cells after (A) 24 h and (B) 48 h, and Balb/3T3 cells after (C) 24 h and (D) 48 h of incubation with UCNPs. (E) Confocal images of HeLa cells after 6 h and 24 h incubation with UCNPs (Scale bars 10 μm). Quantification of UCNPs (F) endocytosed into HeLa cells and (G) exocytosed from HeLa cells after different incubation periods.

comparison to the negatively charged cell membranes. For UCNP@DMSA, the luminescence signals from the particles were observed to progressively increase with incubation time and become more intense than for UCNP@AET after 24 h of incubation (Fig. 5E). This confirms the better protection of UCNPs provided by the DMSA coating compared to AET. Conversely, PEGylated nanostructures showed initially lower fluorescent signals within the cells, originated from the stealth properties of the PEG coating layer hindering interactions with cells and, thus, leading to lower uptakes. Nevertheless, once internalized, this type of UCNPs was well preserved within the cells, as denoted by the luminescence signals observed after 24 h of incubation. On the other hand, UCNP@PMA were initially internalized at similar degree than UCNP@DMSA, but they remain much more luminescently active inside the cells for longer times, corroborating the excellent protective role provided by this polymeric coating (Fig. 5E). The percentage of HeLa cells with internalized surface coated UCNPs after 6 and 24 h incubation was quantified from the obtained confocal microscopy images, corroborating the previously described observations (Fig. S7 in Supplementary Information).

To confirm previous microscopy observations, the internalization of the different ligand-coated UCNPs inside HeLa cells was quantified by ICP-MS. Fig. 5F shows that the content of UCNP@AET inside cells was large and reached a maximum after 6 h of administration to subsequently decrease in agreement with confocal images. Conversely, internalized UCNP@DMSA reached a maximum inside cells after 24 h of administration to slightly decrease afterwards. A similar pattern was also observed for UCNP@PMA. Regarding UCNP@PEG, they were internalized at lower extents than the other types of UCNPs, which confirmed the stealthiness provided by PEG. Thus, we showed that, although AET coating promotes a rapid internalization of UCNPs within HeLa cells, the low protection provided caused faster degradation, agglomeration, and excretion of the particles. PMA-*g*-dodecyl and DMSA

coatings allowed a more sustained internalization over time and provided the UCNPs with the adequate protection to preserve their luminescence properties inside cells, while PEG modification prevents the internalization of large amounts of UCNPs. On the other hand, despite the existence of works analyzing the cell uptake mechanisms of UCNPs, much fewer studies have addressed the particle's exocytosis fate [55,56]. Here, this study was performed, observing that UCNP@AET were those which were most largely cleared out from HeLa cells to the medium after 6 and 24 h of incubation, followed by UCNP@DMSA and UCNP@PMA, in correlation with internalization data. Thus, the reduction in the luminescence intensity of UCNP@AET can also be attributed to the faster clearance of these UCNPs out of cells (Fig. 5G).

In order to corroborate previous ICP-MS data and confocal microscopy observations, the behavior of UCNP@PMA was also evaluated through TEM images. After 2 h incubation, it can be observed that a reduced number of particles have already been incorporated into the cells within endosomes. These endosomes began to break and release the particles into the cytoplasm of the cells after 12 h, while the excretion of these UCNP@PMA from cells in the form of exosomes can be noticed after 24 h. In a high-zoom image after 48 h incubation, it can be observed that the amount of UCNP@PMA internalized within cells remains high, in concordance with previous data, but they begin to aggregate (Fig. S8 in Supplementary Information).

In this way, the performed *in vitro* study confirmed PMA-*g*-dodecyl coating as the best functionalization strategy in view of the potential biomedical application of the designed UCNPs. In concordance with their previously demonstrated high stability and resistance to degradation, UCNP@PMA were those that showed a better compromise between low cytotoxicity degrees, large and constant/steady cellular internalizations, and high preservation of their luminescence properties within cells overtime. PEG coating was highly effective to avoid UCNPs degradation within cells and the derived toxic effects, but it failed to promote the cellular internalization of large number of particles, while DMSA and, specially, AET coatings were not effective to prevent adverse toxic effects to cells.

4. Conclusions

In this work, we synthesized β-hexagonal crystalline UCNPs by the thermal decomposition methodology. The UCNPs were rendered dispersible in aqueous media through their successful surface coating with four different ligands: AET, DMSA, PEG and PMA-*g*-dodecyl. The colloidal stability, degradation, and *in vitro* behavior of the functionalized UCNPs were carefully evaluated, being observed that PEG and, particularly, PMA-*g*-dodecyl coatings provided excellent protection to the nanoparticles while rendered them non-toxic in the analyzed range of concentrations (up to 145 $\mu g \cdot mL^{-1}$). Moreover, PMA-*g*-dodecyl coating allowed a progressive cell internalization of UCNPs within endosomes that began to break and release the particles into the cytoplasm after 12 h incubation, while the onset of UCNPs' excretion from cells within exosomes was observed after 24 h.

Through the performed study, we aimed to establish a real and effective comparison between the four discussed functionalization strategies. It is well-known that small changes on the physicochemical properties of nanoparticles such as size, shape and/or composition directly influence their biological performance, but surface coating is the key player that dictates the biological fate of nanoparticles and, thus, their potential application in the biomedical area. From previous reported works it is quite difficult to decipher which is the more suitable coating for biological application of UCNPs, since the core characteristics of the synthesized nanostructures is largely changed between the different studies. Thus, herein we analyzed the univocal effect of surface coating on the biological fate of UCNPs, observing that the functionalization with PMA-*g*-dodecyl constitutes the most efficient coating strategy. The mechanism used to attach the polymeric molecules appears to be the key factor for the better biological performance of these functionalized UCNPs. Unlike the other three evaluated coatings, here the original OA chains remained on the surface of the particles, resulting in their lower non-radiative quenching in aqueous environments and protecting them from medium-related degradation [23].

From the obtained results, it can be concluded that the evaluation of UCNPs in a wide range of biological conditions (*e.g.* different dispersion media, cell incubation times, *etc.*) constitutes an essential step to determine the best surface functionalization route. Here, the analysis of the behavior of UCNPs in different physiologically-relevant buffers, together with the determination of their *in vitro* performance, was done upon relatively long incubation times compared to many previous studies in which such evaluation was done at shorter time scale (2–24 h) [57–59]. This allowed us to determine the low biological suitability of DMSA and, especially, AET coatings for the long term, despite the former ligands appear as suitable functionalization strategies at shorter incubation times.

In the basis of our present results and some other previous works that carefully evaluated the *in vivo* biocompatibility of UCNPs [60], as well as the negligible concerns related to the biological fate of PMA-based coated nanoparticles [61], we expect that the combination of UCNPs with PMA-*g*-dodecyl coatings render rare-earth-based nanoplatforms with important impact in biomedical applications.

CRediT authorship contribution statement

Lilia Arellano: Writing – original draft, Methodology, Investigation, Conceptualization. **Raquel Martínez:** Writing – review & editing, Formal analysis, Data curation, Conceptualization. **Alberto Pardo:** Writing – review & editing, Investigation, Formal analysis, Data curation, Conceptualization. **Iago Diez:** Writing – original draft, Conceptualization. **Brenda Velasco:** Formal analysis, Data curation. **Antonio Moreda-Piñeiro:** Methodology, Investigation. **Pilar Bermejo-Barrera:** Methodology, Investigation. **Silvia Barbosa:** Project administration, Funding acquisition, Formal analysis, Data curation. **Pablo Taboada:** Writing – review & editing, Project administration, Funding acquisition, Formal analysis, Data curation.

Declaration of competing interest

The authors declare that they have no known competing financial interests or personal relationships that could have appeared to influence the work reported in this paper.

Data availability

Data will be made available on request.

Acknowledgements

This research was funded by Agencia Estatal de Investigación (project number PID2019-109517RB-I00), and Xunta de Galicia (ED431C 2022/18 and ED481B2019/025). ERDF funds are also acknowledged. The authors thank Dr. Ramón Rial (Univ. Santiago de Compostela) for his help editing the figures.

Appendix A. Supplementary data

Supplementary data to this article can be found online at https://doi.org/10.1016/j.jcis.2024.04.188.

References

[1] G. Jalani, V. Tam, F. Vetrone, M. Cerruti, Seeing, Targeting and Delivering with Upconverting Nanoparticles, J Am Chem Soc 140 (2018) 10923–10931, https://doi.org/10.1021/jacs.8b03977.

[2] S. Wen, J. Zhou, K. Zheng, A. Bednarkiewicz, X. Liu, D. Jin, Advances in highly doped upconversion nanoparticles, Nat Commun 9 (2018) 1–12, https://doi.org/10.1038/s41467-018-04813-5.
[3] B. Chen, F. Wang, Emerging Frontiers of Upconversion Nanoparticles, Trends Chem 2 (2020) 427–439, https://doi.org/10.1016/j.trechm.2020.01.008.
[4] E.M. Mettenbrink, W. Yang, S. Wilhelm, Bioimaging with Upconversion Nanoparticles, Adv Photonics Res (2022) 2200098. Doi: 10.1002/ADPR.202200098.
[5] F.K. Kanodarwala, S. Moret, X. Spindler, C. Lennard, C. Roux, Novel upconverting nanoparticles for fingermark detection, Opt Mater (amst) 111 (2021) 110568, https://doi.org/10.1016/j.optmat.2020.110568.
[6] D. Liu, J. Yan, K. Wang, Y. Wang, G. Luo, Continuous synthesis of ultrasmall core-shell upconversion nanoparticles via a flow chemistry method, Nano Res 15 (2022) 1199–1204, https://doi.org/10.1007/s12274-021-3625-3.
[7] Y.H. Chien, K.K. Chan, S.H.K. Yap, K.T. Yong, NIR-responsive nanomaterials and their applications; upconversion nanoparticles and carbon dots: a perspective, Journal of Chemical Technology and Biotechnology 93 (2018) 1519–1528, https://doi.org/10.1002/jctb.5581.
[8] S.F. Himmelstoß, T. Hirsch, A critical comparison of lanthanide based upconversion nanoparticles to fluorescent proteins, semiconductor quantum dots, and carbon dots for use in optical sensing and imaging, Methods Appl Fluoresc 7 (2019) 022002, https://doi.org/10.1088/2050-6120/ab0bfa.
[9] J. Wang, T. Sheng, X. Zhu, Q. Li, Y. Wu, J. Zhang, J. Liu, Y. Zhang, Spectral engineering of lanthanide-doped upconversion nanoparticles and their biosensing applications, Mater Chem Front 5 (2021) 1743–1770, https://doi.org/10.1039/d0qm00910e.
[10] R. Rafique, S.K. Kailasa, T.J. Park, Recent advances of upconversion nanoparticles in theranostics and bioimaging applications, TrAC - Trends in Analytical Chemistry 120 (2019) 115646, https://doi.org/10.1016/j.trac.2019.115646.
[11] A.A. Ansari, A.K. Parchur, G. Chen, Surface modified lanthanide upconversion nanoparticles for drug delivery, cellular uptake mechanism, and current challenges in NIR-driven therapies, Coord Chem Rev 457 (2022) 214423, https://doi.org/10.1016/j.ccr.2022.214423.
[12] M. Huo, P. Liu, L. Zhang, C. Wei, L. Wang, Y. Chen, J. Shi, Upconversion Nanoparticles Hybridized Cyanobacterial Cells for Near-Infrared Mediated Photosynthesis and Enhanced Photodynamic Therapy, Adv Funct Mater 31 (2021) 2010196, https://doi.org/10.1002/adfm.202010196.
[13] A. Gnach, T. Lipinski, A. Bednarkiewicz, J. Rybka, J.A. Capobianco, Upconverting nanoparticles: Assessing the toxicity, Chem Soc Rev 44 (2015) 1561–1584, https://doi.org/10.1039/c4cs00177j.
[14] M.F. Torresan, A. Wolosiuk, Critical Aspects on the Chemical Stability of NaYF4-Based Upconverting Nanoparticles for Biomedical Applications, ACS Appl Bio Mater 4 (2021) 1191–1210, https://doi.org/10.1021/acsabm.0c01562.
[15] R. Li, Z. Ji, C.H. Chang, D.R. Dunphy, X. Cai, H. Meng, H. Zhang, B. Sun, X. Wang, J. Dong, S. Lin, M. Wang, Y.P. Liao, C.J. Brinker, A. Nel, T. Xia, Surface interactions with compartmentalized cellular phosphates explain rare earth oxide nanoparticle hazard and provide opportunities for safer design, ACS Nano 8 (2014) 1771–1783, https://doi.org/10.1021/nn406166n.
[16] R. Li, Z. Ji, J. Dong, C.H. Chang, X. Wang, B. Sun, M. Wang, Y.P. Liao, J.I. Zink, A. E. Nel, T. Xia, Enhancing the imaging and biosafety of upconversion nanoparticles through phosphonate coating, ACS Nano 9 (2015) 3293–3306, https://doi.org/10.1021/acsnano.5b00439.
[17] H.B. Harvey, V. Gowda, G. Cheng, Gadolinium Deposition Disease: A New Risk Management Threat, Journal of the American College of Radiology 17 (2020) 546–550, https://doi.org/10.1016/j.jacr.2019.11.009.
[18] K.T. Rim, K.H. Koo, J.S. Park, Toxicological evaluations of rare earths and their health impacts to workers: A literature review, Saf Health Work 4 (2013) 12–26, https://doi.org/10.5491/SHAW.2013.4.1.12.
[19] D. Lisjak, O. Plohl, J. Vidmar, B. Majaron, M. Ponikvar-Svet, Dissolution Mechanism of Upconverting AYF4:Yb, Tm (A = Na or K) Nanoparticles in Aqueous Media, Langmuir 32 (2016) 8222–8229, https://doi.org/10.1021/acs.langmuir.6b02675.
[20] A. Sedlmeier, H.H. Gorris, Surface modification and characterization of photon-upconverting nanoparticles for bioanalytical applications, Chem Soc Rev 44 (2015) 1526–1560, https://doi.org/10.1039/c4cs00186a.
[21] O. Plohl, S. Kralj, B. Majaron, E. Fröhlich, M. Ponikvar-Svet, D. Makovec, D. Lisjak, Amphiphilic coatings for the protection of upconverting nanoparticles against dissolution in aqueous media, Dalton Transactions 46 (2017) 6975–6984, https://doi.org/10.1039/c7dt00529f.
[22] U. Kostiv, V. Lobaz, J. Kučka, P. Švec, O. Sedláček, M. Hrubý, O. Janoušková, P. Francová, V. Kolářová, L. Šefc, D. Horák, A simple neridronate-based surface coating strategy for upconversion nanoparticles: Highly colloidally stable 125I-radiolabeled NaYF4:Yb3+/Er3+@PEG nanoparticles for multimodal in vivo tissue imaging, Nanoscale 9 (2017) 16680–16688, https://doi.org/10.1039/c7nr05456d.
[23] S. Wilhelm, M. Kaiser, C. Würth, J. Heiland, C. Carrillo-Carrion, V. Muhr, O. S. Wolfbeis, W.J. Parak, U. Resch-Genger, T. Hirsch, Water dispersible upconverting nanoparticles: Effects of surface modification on their luminescence and colloidal stability, Nanoscale 7 (2015) 1403–1410, https://doi.org/10.1039/c4nr05954a.
[24] M.I. Saleh, B. Rühle, S. Wang, J. Radnik, Y. You, U. Resch-Genger, Assessing the protective effects of different surface coatings on NaYF4:Yb3+, Er3+ upconverting nanoparticles in buffer and DMEM, Sci Rep 10 (2020) 1–11, https://doi.org/10.1038/s41598-020-76116-z.
[25] Y.F. Wang, L.D. Sun, J.W. Xiao, W. Feng, J.C. Zhou, J. Shen, C.H. Yan, Rare-earth nanoparticles with enhanced upconversion emission and suppressed rare-earth-ion leakage, Chemistry - A European Journal 18 (2012) 5558–5564, https://doi.org/10.1002/chem.201103485.
[26] D. Valdeperez, N. Wutke, L.M. Ackermann, W.J. Parak, M. Klapper, B. Pelaz, Colloidal stability of polymer coated zwitterionic Au nanoparticles in biological media, Inorganica Chim Acta 534 (2022) 120820, https://doi.org/10.1016/j.ica.2022.120820.
[27] A. Pardo, S. Yáñez, Y. Piñeiro, R. Iglesias-Rey, A. Al-Modlej, S. Barbosa, J. Rivas, P. Taboada, Cubic Anisotropic Co- and Zn-Substituted Ferrite Nanoparticles as Multimodal Magnetic Agents, ACS Appl Mater Interfaces 12 (2020) 9017–9031, https://doi.org/10.1021/acsami.9b20496.
[28] A. Pardo, B. Pelaz, J. Gallo, M. Bañobre-López, W.J. Parak, S. Barbosa, P. del Pino, P. Taboada, Synthesis, Characterization, and Evaluation of Superparamagnetic Doped Ferrites as Potential Therapeutic Nanotools, Chemistry of Materials 32 (2020) 2220–2231, https://doi.org/10.1021/acs.chemmater.9b04848.
[29] R. Martínez, E. Polo, S. Barbosa, P. Taboada, P. Del Pino, B. Pelaz, 808 Nm-Activable Core@Multishell Upconverting Nanoparticles With Enhanced Stability for Efficient Photodynamic Therapy, J Nanobiotechnology 18 (2020) 1–15, https://doi.org/10.1186/s12951-020-00640-3.
[30] A. Pardo, R. Pujales, M. Blanco, E.M. Villar-Alvarez, S. Barbosa, P. Taboada, V. Mosquera, Analysis of the influence of synthetic paramaters on the structure and physico-chemical properties of non-spherical iron oxide nanocrystals and their biological stability and compatibility, Dalton Transactions 45 (2015) 797–810, https://doi.org/10.1039/c5dt03923a.
[31] Z. Shi, Y. Duan, X. Zhu, Q. Wang, D. Li, K. Hu, W. Feng, F. Li, C. Xu, Dual functional NaYF4:Yb3+, Er3+@NaYF4:Yb3+, Nd3+ core-shell nanoparticles for cell temperature sensing and imaging, Nanotechnology 29 (2018) 094001, https://doi.org/10.1088/1361-6528/aaa44a.
[32] D. Tu, L. Liu, Q. Ju, Y. Liu, H. Zhu, R. Li, X. Chen, Time-resolved FRET biosensor based on amine-functionalized lanthanide-doped NaYF4 nanocrystals, Angewandte Chemie - International Edition 50 (2011) 6306–6310, https://doi.org/10.1002/anie.201100303.
[33] Z. Li, Y. Zhang, An efficient and user-friendly method for the synthesis of hexagonal-phase NaYF4:Yb, Er/Tm nanocrystals with controllable shape and upconversion fluorescence, Nanotechnology 19 (2008) 345606, https://doi.org/10.1088/0957-4484/19/34/345606.
[34] H.S. Qian, Y. Zhang, Synthesis of hexagonal-phase core-shell NaYF4 nanocrystals with tunable upconversion fluorescence, Langmuir 24 (2008) 12123–12125, https://doi.org/10.1021/la802343f.
[35] J. Hühn, C. Carrillo-Carrion, M.G. Soliman, C. Pfeiffer, D. Valdeperez, A. Masood, I. Chakraborty, L. Zhu, M. Gallego, Z. Yue, M. Carril, N. Feliu, A. Escudero, A. M. Alkilany, B. Pelaz, P. Del Pino, W.J. Parak, Selected standard protocols for the synthesis, phase transfer, and characterization of inorganic colloidal nanoparticles, Chemistry of Materials 29 (2017) 399–461, https://doi.org/10.1021/acs.chemmater.6b04738.
[36] D. Baziulyte-Paulaviciene, N. Traskina, R. Vargalis, A. Katelnikovas, S. Sakirzanovas, Thermal decomposition synthesis of Er3+-activated NaYbF4 upconverting microparticles for optical temperature sensing, J Lumin 215 (2019) 116672, https://doi.org/10.1016/j.jlumin.2019.116672.
[37] H. Na, K. Woo, K. Lim, H.S. Jang, Rational morphology control of β-NaYF4:Yb, Er/tm Upconversion Nanophosphors Using a Ligand, an Additive, and Lanthanide Doping, Nanoscale 5 (2013) 4242–4251, https://doi.org/10.1039/c3nr00080j.
[38] X. Zhu, J. Zhang, J. Liu, Y. Zhang, Recent Progress of Rare-Earth Doped Upconversion Nanoparticles: Synthesis, Optimization, and Applications, Advanced Science 6 (2019) 1901358, https://doi.org/10.1002/advs.201901358.
[39] Y. Shang, S. Hao, J. Liu, M. Tan, N. Wang, C. Yang, G. Chen, Synthesis of upconversion β-NaYF 4: Nd 3+ /Yb 3+ /Er 3+ particles with enhanced luminescent intensity through control of morphology and phase, Nanomaterials 5 (2014) 218–232, https://doi.org/10.3390/nano5010218.
[40] A. Sedlmeier, D.E. Achatz, L.H. Fischer, H.H. Gorris, O.S. Wolfbeis, Photon upconverting nanoparticles for luminescent sensing of temperature, Nanoscale 4 (2012) 7090–7096, https://doi.org/10.1039/c2nr32314a.
[41] S.K. Seol, D. Kim, S. Jung, W.S. Chang, J.T. Kim, One-step synthesis of PEG-coated gold nanoparticles by rapid microwave heating, J Nanomater 2013 (2013) 531760, https://doi.org/10.1155/2013/531760.
[42] J. Lee, Y.H. Choa, J. Kim, K.H. Kim, Comparison of the Magnetic Properties for the Surface-Modified Magnetite Nanoparticles, IEEE Trans Magn 47 (2011) 2874–2877, https://doi.org/10.1109/TMAG.2011.2145414.
[43] A.K. Gupta, S. Wells, Surface-Modified Superparamagnetic Nanoparticles for Drug Delivery: Preparation, Characterization, and Cytotoxicity Studies, IEEE Trans Nanobioscience 3 (2004) 66–73, https://doi.org/10.1109/TNB.2003.820277.
[44] J.Y. Park, P. Daksha, G.H. Lee, S. Woo, Y. Chang, Highly Water-Dispersible PEG Surface modified Ultra Small Superparamagnetic iron Oxide Nanoparticles Useful for Target-Specific Biomedical Applications, Nanotechnology 19 (2008) 365603, https://doi.org/10.1088/0957-4484/19/36/365603.
[45] N.Y. Siavashi, B. Akhlaghinia, M. Zarghani, Sulfonated nanohydroxyapatite functionalized with 2-aminoethyl dihydrogen phosphate (HAP@AEPH2-SO3H) as a reusable solid acid for direct esterification of carboxylic acids with alcohols, Research on Chemical Intermediates 42 (2016) 5789–5806, https://doi.org/10.1007/s11164-015-2404-8.
[46] B. Pelaz, P. Del Pino, P. Maffre, R. Hartmann, M. Gallego, S. Rivera-Fernández, J. M. De La Fuente, G.U. Nienhaus, W.J. Parak, Surface Functionalization of Nanoparticles with Polyethylene Glycol: Effects on Protein Adsorption and Cellular Uptake, ACS Nano 9 (2015) 6996–7008, https://doi.org/10.1021/acsnano.5b01326.
[47] A.M. Aldosari, E.S. Akpata, N. Khan, Associations among Dental Caries Experience, Fluorosis, and Fluoride Exposure from Drinking Water Sources in Saudi Arabia,

J Public Health Dent 70 (2010) 220–226, https://doi.org/10.1111/j.1752-7325.2010.00169.x.
[48] P.D. Beer, P.A. Gale, Anion Recognition and Sensing: the State of the Art and Future Perspectives, Angewandte Chemie - International Edition 40 (2001) 486–516, https://doi.org/10.1002/1521-3773(20010202)40:3<486::AID-ANIE486>3.0.CO;2-P.
[49] E. Andresen, C. Würth, C. Prinz, M. Michaelis, U. Resch-Genger, Time-resolved luminescence spectroscopy for monitoring the stability and dissolution behaviour of upconverting nanocrystals with different surface coatings, Nanoscale 12 (2020) 12589–12601, https://doi.org/10.1039/d0nr02931a.
[50] L.E. Mackenzie, J.A. Goode, A. Vakurov, P.P. Nampi, S. Saha, G. Jose, P.A. Millner, The theoretical molecular weight of NaYF 4:RE upconversion nanoparticles, Sci Rep 8 (2018) 1–11, https://doi.org/10.1038/s41598-018-19415-w.
[51] S. Lahtinen, A. Lyytikäinen, H. Päkkilä, E. Hömppi, N. Perälä, M. Lastusaari, T. Soukka, Disintegration of hexagonal NaYF4:Yb3+, Er3+ upconverting nanoparticles in aqueous media: The role of fluoride in solubility equilibrium, Journal of Physical Chemistry C 121 (2017) 656–665, https://doi.org/10.1021/acs.jpcc.6b09301.
[52] O. Plohl, M. Kraft, J. Kovač, B. Belec, M. Ponikvar-Svet, C. Würth, D. Lisjak, U. Resch-Genger, Optically detected degradation of NaYF4:Yb, Tm-based upconversion nanoparticles in phosphate buffered saline solution, Langmuir 33 (2017) 553–560, https://doi.org/10.1021/acs.langmuir.6b03907.
[53] S.F. Himmelstoß, T. Hirsch, Long-Term Colloidal and Chemical Stability in Aqueous Media of NaYF4-Type Upconversion Nanoparticles Modified by Ligand-Exchange, Particle and Particle Systems Characterization 36 (2019) 1900235, https://doi.org/10.1002/ppsc.201900235.
[54] W. Lv, J. Ye, Q. Wang, C. Li, J. Wang, Z. Zhang, N. Niu, Z. Liu, J. Xu, Y. Fu, Tumor-Responsive Upconversion Nanoparticles with Tunable Degradability and Ultrabright Emission for Optical Bioimaging, ACS Appl Nano Mater 5 (2022) 9367–9378, https://doi.org/10.1021/acsanm.2c01670.
[55] Y.M. Bae, Y. Il Park, S.H. Nam, J.H. Kim, K. Lee, H.M. Kim, B. Yoo, J.S. Choi, K. T. Lee, T. Hyeon, Y.D. Suh, Endocytosis, intracellular transport, and exocytosis of lanthanide-doped upconverting nanoparticles in single living cells, Biomaterials 33 (2012) 9080–9086, https://doi.org/10.1016/j.biomaterials.2012.08.039.
[56] Y.H. Song, R. De, K.T. Lee, Uptake of polyelectrolyte functionalized upconversion nanoparticles by tau-aggregated neuron cells, Pharmaceutics 13 (2021) 1–12, https://doi.org/10.3390/pharmaceutics13010102.
[57] S. Wang, L. Zhang, C. Dong, L. Su, H. Wang, J. Chang, Smart pH-Responsive Upconversion Nanoparticles for Enhanced Tumor Cellular Internalization and Near-Infrared Light-Triggered Photodynamic Therapy, Chemical Communications 51 (2015) 406–408, https://doi.org/10.1039/c4cc08178a.
[58] E. Voronovic, A. Skripka, G. Jarockyte, M. Ger, D. Kuciauskas, A. Kaupinis, M. Valius, R. Rotomskis, F. Vetrone, V. Karabanovas, Uptake of Upconverting Nanoparticles by Breast Cancer Cells: Surface Coating versus the Protein Corona, ACS Appl Mater Interfaces 13 (2021) 39076–39087, https://doi.org/10.1021/acsami.1c10618.
[59] H.S. Park, J. Kim, M.Y. Cho, Y.J. Cho, Y.D. Suh, S.H. Nam, K.S. Hong, Effectual Labeling of Natural Killer Cells with Upconverting Nanoparticles by Electroporation for in Vivo Tracking and Biodistribution Assessment, ACS Appl Mater Interfaces 12 (2020) 49362–49370, https://doi.org/10.1021/acsami.0c12849.
[60] C. Liu, H. Shao, D. Li, X. Sui, N. Liu, S.U. Rahman, X. Li, P.R. Arany, Safety and efficacy of citric acid-upconverting nanoparticles for multimodal biological imaging in BALB/c mice, Photodiagnosis Photodyn Ther 36 (2021) 102485, https://doi.org/10.1016/J.PDPDT.2021.102485.
[61] M. Xu, M.G. Soliman, X. Sun, B. Pelaz, N. Feliu, W.J. Parak, S. Liu, How entanglement of different physicochemical properties complicates the prediction of in vitro and in vivo interactions of gold nanoparticles, ACS Nano 12 (2018) 10104–10113, https://doi.org/10.1021/ACSNANO.8B04906/SUPPL_FILE/NN8B04906_SI_002.XLSX.
[63] V. Figueroa, B. Velasco, L. Arellano, V. Domínguez-Arca, A. Cambón, A. Pardo, A. Topete, L.C. Rosales-Rivera, J.F. Armando Soltero, S. Barbosa, P. Taboada, Role of surface functionalization and biomolecule structure on protein corona adsorption and conformation onto anisotropic metallic nanoparticles, J Mol Liq 398 (2024) 124240, https://doi.org/10.1016/j.molliq.2024.124240.